Food Chemistry: X 20 (2023) 100954

Contents lists available at ScienceDirect

Food Chemistry: X

journal homepage: www.sciencedirect.com/journal/food-chemistry-x

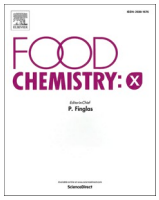

Improvement of emulsifying stability of coconut globulin by noncovalent interactions with coffee polyphenols

Yile Chen [a,1], Yang Chen [a,1], Lianzhou Jiang [a,c], Zhaoxian Huang [a], Weimin Zhang [a,b,*], Yonghuan Yun [a,*]

[a] School of Food Science and Engineering, Hainan University, Haikou 570228, China
[b] Key Laboratory of Tropical Fruits and Vegetables Quality and Safety for State Market Regulation, Hainan Institute for Food Control, Haikou, Hainan 570228, China
[c] College of Food Science, Northeast Agricultural University, Harbin, Heilongjiang 150030, China

ARTICLE INFO

Keywords:
Coconut globulin
Coffee polyphenol
Hydrogen bond
Interfacial film
Stability

ABSTRACT

Coconut milk is an unstable emulsion system, mainly stabilized by proteins, which limits the development of the food industry. The aim of this study was to investigate mechanisms for increasing emulsion stability through the interaction between coffee polyphenols (CPs) and coconut globulin (CG), the main protein in coconut milk. Caffeic acid (CA), chlorogenic acid (CHA), and ferulic acid (FA) were selected as CP models. The results showed that hydrogen bond interactions mainly occurred between CG and CPs (CG-FA < CG-CA < CG-CHA). CHA containing quinic acid preferentially formed a strong interaction with CG. The interaction changed the lipophilicity of CG and facilitated the formation of a dense and thick interfacial film at the oil–water interface. Furthermore, the emulsion stabilized by CG-CPs showed excellent stability after storage, centrifugation, pH, and salt treatment, especially CG-CHA. This study could provide a theoretical basis for improving the stability of coconut milk products.

Introduction

Coconut milk, obtained from crushing, squeezing, and extracting mature coconut meat, is nutrient-dense and rich in fats, proteins, minerals, and vitamins (Zhao et al., 2023). Coconut milk consists of 31.0–35.0 % fat and 3.5–4.0 % protein (Zhao et al., 2023). Coconut protein, an amphiphilic molecule, can be adsorbed, unfolded and rearranged at the oil–water (O/W) interface, stabilizing the oil-in-water emulsion (Chen et al., 2023a). Due to its high nutritional value and unique taste, it is widely used in drinks, ice cream, and cooking. However, coconut milk, like other emulsions, represents a thermodynamically unstable system (Chen, Chen, Fang, Pei, & Zhang, 2024). Since coconut protein has limited emulsifiability, droplets of coconut milk without emulsifiers easily agglomerate and aggregate, therefore tending to phase separate (Tangsuphoom & Coupland, 2009).

The most common method to improve the stability of coconut milk is to add emulsifiers, surfactants, and thickeners, such as protein, sorbitol esters, ethoxy esters, and sucrose esters (Ariyaprakai, Limpachoti, & Pradipasena, 2013). However, for safety reasons, the amount of these additives is limited. Previous research suggests that the stability of coconut milk can be improved by adding natural proteins (improves emulsification) and starch (increases viscosity) (Arlai & Tananuwong, 2021; Tangsuphoom & Coupland, 2009). Nevertheless, the addition of protein and starch can affect the taste and flavor of coconut milk, which is determined by the delicate balance of flavors fat, protein, and carbohydrates.

Coconut milk contains proteins such as albumin, globulin, glutenin, and gliadin, with globulin and albumin serving as emulsifiers to stabilize the coconut milk emulsion (Tangsuphoom & Coupland, 2008). In coconut milk, coconut globulin (CG) is the most abundant protein and the one with the highest emulsifying capacity (Kwon, Park, & Rhee, 1996). Our previous work demonstrated that CG can be oxidized by cold plasma to improve emulsifying properties (Chen et al., 2023c). Furthermore, changing environmental factors (pH and temperature) can adjust the emulsifying properties of CG (Ma et al., 2023). Therefore, modification of CG can improve its emulsifying properties, thereby enhancing the stability of coconut milk.

Protein modification through interactions with other food

* Corresponding authors at: School of Food Science and Engineering, Hainan University, Haikou, Hainan 570228, China.
E-mail addresses: zhwm1979@163.com (W. Zhang), yunyonghuan@foxmail.com (Y. Yun).
[1] These authors contribute equally to the work.

https://doi.org/10.1016/j.fochx.2023.100954
Received 20 September 2023; Received in revised form 16 October 2023; Accepted 19 October 2023
Available online 21 October 2023

components such as polyphenols has been identified as a promising strategy to improve the functional properties of protein (Li et al., 2021). Phenolic compounds, possessing at least one aromatic ring and one or more hydroxyl groups, are natural antioxidants (Ma et al., 2023). Polyphenols can interact with proteins through covalent/noncovalent interactions. Covalent interactions are based on the oxidation of polyphenols and nucleophilic addition, while noncovalent interactions include hydrogen bonds, hydrophobic interactions, and electrostatic interactions (Li et al., 2021). These interactions can be exploited in emulsion-based food systems to improve the oxidative stability of the product, as demonstrated in products such as milk and soy milk (Li et al., 2021). Therefore, considering the interaction between CG and polyphenols could promote the adsorption of protein molecules at the O/W interface, thereby improving emulsifying stability.

Coffee, one of the most popular beverages worldwide, is rich in polyphenols such as caffeic acid (CA), chlorogenic acid (CHA), and ferulic acid (FA), which have potential antioxidant, hypoglycemic, antihypertensive, antibacterial, and anti-inflammatory effects (Bondam, da Silveira, dos Santos, & Hoffmann, 2022). Additionally, certain studies have demonstrated that coffee polyphenols (CPs) such as CA and CHA can interact with proteins to enhance their functional properties (Qi et al., 2023). However, the mechanisms by which different CPs improve protein emulsifying properties remain unclear.

In this study, CA, CHA, and FA were selected as CP models to investigate the mechanism by which different CPs improve the emulsifying properties of CG. Thermodynamic parameters and molecular docking were used to determine the interaction between CA, CHA, FA, and CG. Methods such as sodium dodecyl sulfate–polyacrylamide gel electrophoresis (SDS-PAGE), circular dichroism (CD) spectroscopy, fourier transform infrared (FTIR) spectroscopy, and fluorescence spectroscopy were employed to characterize the impact of the interaction between CPs and CG on protein structure. The interfacial tension and emulsifying activity of CG-CPs were observed. Finally, the storage stability, centrifugal stability, pH stability, and salt stability of the prepared emulsion were characterized.

Materials and methods

Materials

Caffeic acid (≥99 %, molecular weight 180.15 Da), chlorogenic acid (≥98 %, molecular weight 354.21 Da), and ferulic acid (≥98 %, molecular weight 194.18 Da) were purchased from Shanghai Deepak Biotechnology Co., Ltd. (Shanghai, China). Soybean oil (food grade) was purchased from China Grain and Oil Food Co., Ltd. (Beijing, China). All other reagents were of analytical grade and purchased from Aladdin Co., Ltd. (Shanghai, China).

Preparation of CG

The extraction of CG was carried out according to the procedure described by Chen et al. (2023c). Coconut was obtained from Wenchang, Hainan Province, and used for extraction. The oil was removed from the freeze-dried coconut meat powder with *n*-hexane, and CG was extracted with 0.5 mol/L NaCl solution at a ratio of 1:5 (w/v) for 4 h. The extract was then freeze-dried and stored at 4 °C.

Preparation of CG and CG-CPs complexes

The CG was dissolved in 0.01 mol/L phosphate buffer solution (PBS, pH 6.0), stirred for 2 h, and left overnight for complete hydration, achieving a final solution concentration of 2.0 mg/mL. CA, CHA, and FA were each dissolved in 0.01 mol/L PBS (pH 6.0) to a concentration of 2.0 mg/mL. The solutions of CA, CHA, and FA were added dropwise to the CG solution, stirring equal volumes at low speed to ensure sufficient reaction. The pH of all samples was adjusted to 6.0 using 0.1 mol/L HCl and 0.1 mol/L NaOH solutions to match the pH of commercial coconut milk products (≥5.9) (Zhao et al., 2023). The solutions were labeled as CG-CA, CG-CHA, and CG-FA, respectively. The CG solution (1 mg/mL) was used as a control and all samples were stored at 4 °C for short-term storage.

Fluorescence spectrum measurement

The fluorescence spectra were measured using a fluorescence spectrophotometer (F-7000, Hitachi, Japan), according to the method described by Lu et al. (2022). The CG solution was combined with CA, CHA, and FA solutions to prepare samples with a CG concentration of 1 mg/mL in the final complex. The concentrations of CA, CHA, and FA were 0, 20, 40, 60, 80, 100, 120, and 140 μ mol/L, respectively. The interactions within the complexes were analyzed at temperatures of 298, 303, and 308 K. A 0.01 mol/L PBS buffer (pH 6.0) was used as a blank. Intrinsic emission fluorescence spectra of the samples were recorded in the range of 290 to 550 nm at an excitation wavelength of 280 nm. The scanning speed was 1200 nm/min and the slit width was set to 2.5 nm.

Molecular docking simulation

The molecular docking method was used to simulate the binding mode and affinity of polyphenols and CG. The CG ID (5WPW) was entered into the RCSB database (https://www.rcsb.org/) to obtain the CG molecular model. MOE 2012 software was used for preprocessing, which included adding hydrogen atoms, optimizing charge, and removing water molecules. The structures of the polyphenols were obtained from PubChem (https://pubchem.ncbi.nlm.nih.gov). Since the entire protein represents the potential binding site, the conformation with the lowest binding energy was selected as the optimal conformation. The binding site and interaction forces were analyzed.

Determination of CG, CG-CA, CG-CHA and CG-FA structure

SDS-PAGE was performed using a precast Biosharp PAGE gel (Tris-Gly, 4 %–20 %, 10 ×). Samples were prepared by mixing a 1 mg/mL sample solution with loading buffer (SDS-PAGE protein loading buffer, 5 ×) at a volume ratio of 4:1 then heating the mixtures in a water bath at 100 °C for 3–5 min for denaturation. A volume of 10 μL each sample solution was loaded into each well and the voltage was adjusted to 90 V (for the stacking gel)/120 V (for the separating gel). The gel was stained with Coomassie Brilliant Blue R250 and then destained with the destaining solution.

CD spectra were obtained with a Bio-Logic MOS-500 circular dichroism spectrometer (Isere, France) in the 190–250 nm range. Sample solutions were diluted to 0.5 mg/mL, and deionized water, CA, CHA, and FA solutions without CG were used as controls. The spectra were an average of three scans.

The FTIR spectra of the samples were measured using an FTIR spectrometer (TENSOR 27, Bruker, Germany). Freeze-dried powder samples (10 mg) were mixed with KBr at a ratio of 1:100 (w/w) and pressed into tablets. Spectra were recorded in the wavenumber range of 4000–400 cm^{-1} with air as a background. Each FTIR spectrum consisted of 32 scans on average.

The free -SH and S—S bond content of samples were determined as previously reported Chen et al. (2023c). The freeze-dried samples were dissolved in Tris-Gly-urea buffer (0.086 mol/L Tris, 0.090 mol/L glycine, 8 mol/L urea, 0.004 mol/L ethylenediaminetetraacetic acid, pH 8.0) to prepare 6 mg/mL solutions. The supernatant was centrifuged and then 80 μL (4 mg/mL) of 5,5′-Dithio bis-(2-nitrobenzoic acid) (DTNB) was added to 2 mL of supernatant and allowed to react for 5 min at 25 °C. The -SH content was calculated by measuring the absorbance at 412 nm. To determine the S—S bond content, 2 mL of the above supernatant was reacted with β-mercaptoethanol (4 mg) for 2 h at 25 °C. Then, a 12 % trichloroacetic acid solution was added and centrifuged for

1 h, followed by repeated washing and precipitation. After adding 80 μL of the DTNB solution, the absorbance was measured at 412 nm, and the total S—S content was calculated as follows Eqs. (1) and (2):

$$Free-SHcontent(\mu mol/gprotein)=\frac{73.53\times A412\times D}{C} \quad (1)$$

$$S-Sbondcontent(\mu mol/gprotein)=\frac{1}{2}\times(Total-SHcontent-Free-SHcontent) \quad (2)$$

where A_{412} is the absorbance value at 412 nm, D is the dilution ratio, and C is the protein concentration in the sample.

Particle size and zeta potential measurement

Sample solutions (5 mL) were diluted with deionized water to achieve a concentration of 0.5 mg/mL and particle size and zeta potential were measured three times using a Malvern ZS 90 (Malvern Instruments, Malvern, Worcestershire, UK). The temperature was kept constant at 25 °C during measurements.

Turbidity measurement

The turbidity of the samples was determined according to a previously published method (Zheng et al., 2022) with minor modifications. The samples were sufficiently diluted to 0.5 mg/mL, and the absorbance was measured at 600 nm with a UV spectrophotometer (TU-1901, Universal Instruments, Beijing).

Transmission electron microscope (TEM)

The microstructure of the samples was characterized using a transmission electron microscope (JEM-2100, JEOL, Japan). Samples were placed dropwise on a carbon-coated copper grid and stained with drops of uranium acetate to prevent light exposure to light. After drying, the samples were observed under the transmission electron microscope and images were taken.

Determination of CG, CG-CA, CG-CHA and CG-FA properties

Protein solubility was modified by the Bradford method (Chelh, Gatellier, & Sante-Lhoutellier, 2006). The standard solution of bovine serum albumin (BSA) was prepared and a standard curve was recorded. The sample solutions (1 mg/mL) were centrifuged at 8000 r/min for 20 min, and 1 mL of the supernatants was collected to determine the protein concentration. Protein solubility was expressed as protein concentration in the supernatant relative to the protein concentration before centrifugation.

Surface hydrophobicity was determined by the bromophenol blue method. According to Chelh et al. (2006) described procedure, the prepared protein solution (1 mg/mL, 0.1 mL) was diluted to an appropriate concentration, mixed with a 1 mg/mL bromophenol blue solution (20 μL), and centrifuged. The absorbance of the supernatant was measured at 595 nm. The surface hydrophobicity of the protein was indicated by the amount of bromophenol blue bound.

The dynamic interfacial tension was measured at 25 °C using a drop profile tensiometer (OT100, Ningbo NB Scientific Instruments, China). Due to the technical requirements of the tensiometer, samples were sufficiently diluted and each drop volume was maintained at 10 μL while soybean oil was loaded into a syringe. The dynamic interfacial tension was measured for 7200 s until no further change in interfacial tension was observed.

Preparation of emulsions

Refer to the previous method and modify it (Wu, Wu, Lin, & Shao, 2022), CG and CG-CPs solutions were mixed with soybean oil at a volume ratio of 9:1 to obtain a 10 % oil phase mixture with a final CG concentration of 10 mg/mL. These solutions were sheared with a high-speed shearing machine at a speed of 10,000 rpm for 1 min to prepare macroemulsions. These macroemulsions were then processed using a NanoGenzier high-pressure homogenizer (Genizer, USA) at 20 MPa and passed twice to generate microemulsions. The temperature was maintained at approximately 25 °C during shearing to produce oil-in-water emulsions stabilized by CG, CG-CA, CG-CHA, and CG-FA. Subsequently, 0.02 % thiomersal was added to each emulsion to inhibit microbial growth. All emulsions were stored at 4 °C.

Emulsifying activity

Droplet size distribution and average droplet size of the emulsion were measured using a Malvern Master Sizer 2000 instrument (Malvern Instruments, Malvern Hills, UK). For this experiment, the universal spherical analysis model was used and the refractive index of the oil droplets and dispersed water was set to 1.46 and 1.33, respectively, with the obscuration values ranging from 5 % to 15 %.

Viscosity measurements were carried out using a Haake Mars 40 rheometer (Thermo Fisher, USA). The shear rate was gradually increased from 1 to 100 s^{-1} during the measurement while the temperature of the sample (1 mL) was maintained 25 °C. By comparing the flow properties of different samples, the effect of the addition of CPs on the flow properties of the CG-stabilized emulsion was determined. All data provided represents the average of three replicates.

Emulsion stability under different conditions

The droplet morphology of the emulsion after s 0, 7, 14, 21, and 28 days of storage as directly observed with an inverted microscope (Leica Microsystems CMS GmbH, Germany).

The centrifugal stability of the emulsions (0.4 mL) was further analyzed using a LUMiSizer stability analyzer (LUMiSizer, L.U.M. GmbH, Germany). The optical wavelength was set to 870 nm and the optical factor was 1.00. The contour line was set to 300, the time interval to 10 s, and the required time to 50 min.

To evaluate the pH stability of the emulsion, fresh emulsion samples (10 mL) were adjusted to pH 4.0, 5.0, 6.0, 7.0, and 8.0 using 0.1 mol/L HCl and 0.1 mol/L NaOH solutions. The droplet size of the emulsion was measured. The creaming index (CI) of the emulsion was determined using the following Eq. (3):

$$CI(\%)=\frac{HS}{HE}\times 100\% \quad (3)$$

where H_E and H_S represent the total heights of the emulsion and the serum layer of the emulsion, respectively.

Different concentrations of NaCl solution (0.05–0.3 mol/L) were added to the emulsion (10 mL). The emulsion index and the droplet size were determined after 3 h.

Statistical analysis

Three independent experiments were performed for all treatments and the results were expressed as mean ± standard deviation (SD). Data processing and statistical analysis were performed using IBM SPSS Statistics 22. The significance level was set at $p < 0.05$.

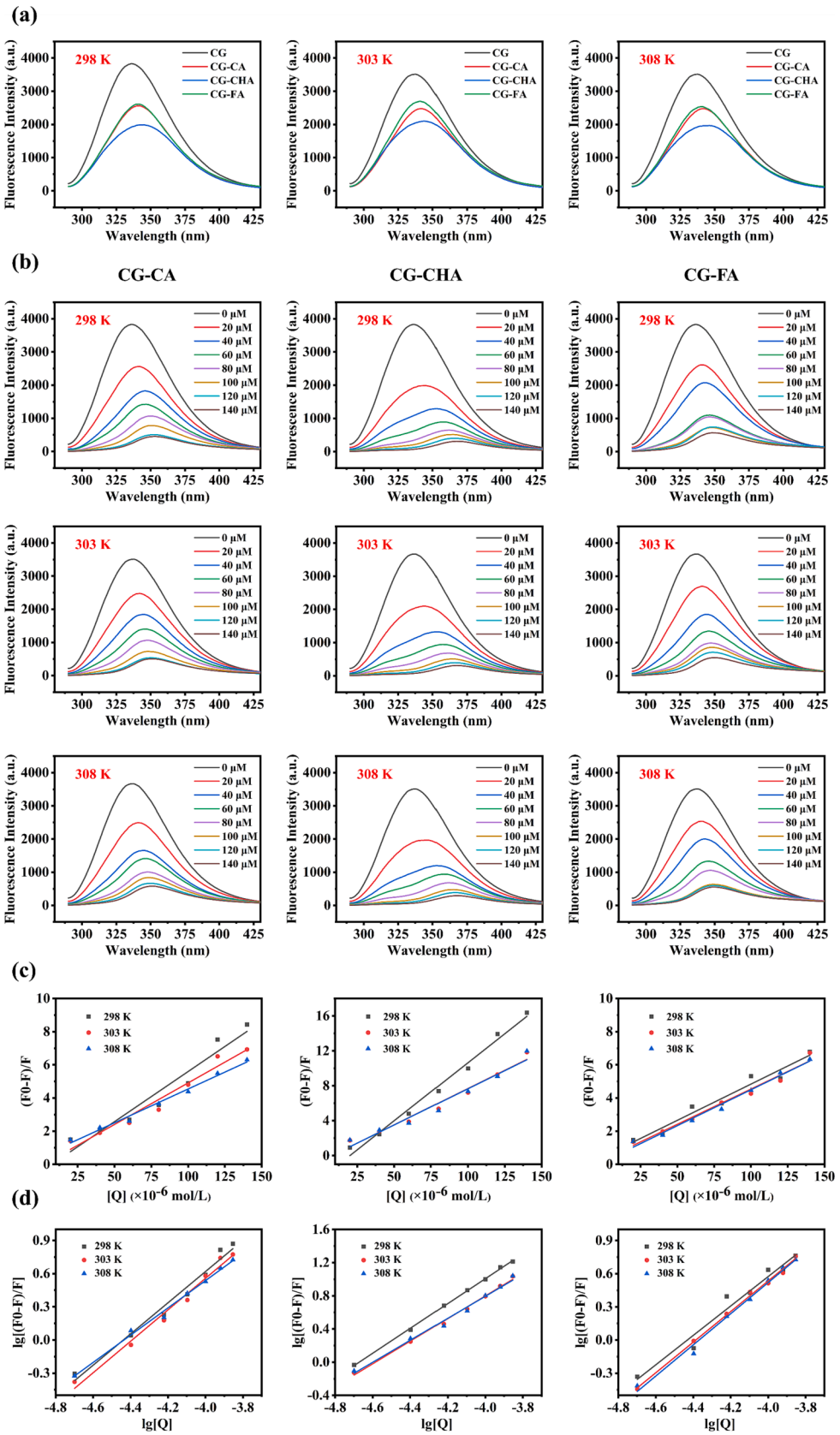

Fig. 1. Fluorescence emission spectra of CG (1 mg/mL) in the presence of 20 μM polyphenols (CA, CHA, and FA) at 298, 303, and 308 K (a); Fluorescence spectra of CG (1 mg/mL) with increasing concentration of CA, CHA, and FA (0–140 μM) at 298, 303, and 308 K (b); Stern-Volmer (c) and double logarithmic plots (d) for the quenching of protein by CA, CHA, and FA at 298, 303, and 308 K.

Table 1
The binding parameters and thermodynamic parameters for the interaction of the CG with CA, CHA and FA.

Sample	T (K)	K_{SV} ($\times 10^4$ L·moL^{-1})	K_q ($\times 10^{12}$ L·moL^{-1}·s^{-1})	R^2	K_a ($\times 10^6$ L·moL^{-1})	n	R^2	ΔH (kJ·moL^{-1})	ΔS (kJ·moL^{-1}·K^{-1})	ΔG (kJ·moL^{-1})
CA-CG	298	6.04 ± 0.007^{d}	6.04 ± 0.007^{d}	0.94	1.82 ± 0.040^{b}	1.41 ± 0.097^{bc}	0.98	−138.05 ± 0.096^{b}	−0.34 ± 0.032^{b}	−36.45 ± 0.027^{f}
	303	5.01 ± 0.005^{e}	5.01 ± 0.005^{e}	0.96	1.78 ± 0.034^{b}	1.42 ± 0.082^{e}	0.98			−34.74 ± 0.009^{c}
	308	4.07 ± 0.002^{g}	4.07 ± 0.002^{g}	0.99	0.30 ± 0.019^{g}	1.23 ± 0.046^{b}	0.99			–33.04 ± 0.010^{a}
CHA-CG	298	13.3 ± 0.007^{a}	13.3 ± 0.007^{a}	0.99	10.23 ± 0.009^{a}	1.50 ± 0.020^{a}	0.99	−158.71 ± 0.071^{c}	−0.40 ± 0.024^{c}	−39.45 ± 0.021^{h}
	303	8.34 ± 0.006^{b}	8.34 ± 0.006^{b}	0.97	1.82 ± 0.017^{b}	1.37 ± 0.041^{cd}	0.99			−37.44 ± 0.024^{g}
	308	8.31 ± 0.007^{c}	8.31 ± 0.007^{c}	0.96	1.29 ± 0.026^{d}	1.33 ± 0.063^{d}	0.99			−35.44 ± 0.011^{e}
FA-CG	298	4.37 ± 0.004^{f}	4.37 ± 0.004^{f}	0.96	0.79 ± 0.048^{f}	1.33 ± 0.115^{d}	0.96	45.76 ± 0.009^{a}	0.27 ± 0.030^{a}	–33.72 ± 0.002^{b}
	303	4.25 ± 0.003^{f}	4.25 ± 0.003^{f}	0.98	1.17 ± 0.016^{e}	1.38 ± 0.037^{bc}	0.99			−35.06 ± 0.012^{d}
	308	4.33 ± 0.002^{f}	4.33 ± 0.002^{f}	0.99	1.45 ± 0.026^{c}	1.41 ± 0.063^{bc}	0.99			−36.39 ± 0.009^{f}

Note: Different letters in the same column indicate significant difference ($p < 0.05$).

Result

Interaction between CG and CPs

As shown in Fig. 1**a-b**, the fluorescence intensity of CG at the excitation wavelength of 280 nm decreased with the introduction of CPs. When polyphenols are introduced into a protein solution containing fluorophores, the fluorescent groups of the protein are disrupted, resulting in a decrease in fluorescence intensity (Condict & Kasapis, 2022). Therefore, it was concluded that the quenching of CG fluorescence intensity was a result of the interaction between CG and CPs.

To determine the type of quenching, the fluorescence emission spectrum data were processed using the Stern-Volmer equation at temperatures of 298, 303, and 308 K (Condict et al., 2022):

$$\frac{F0}{F} = 1 + Kq\tau 0[Q] = 1 + KSV[Q]\frac{F0}{F} = 1 + Kq\tau 0[Q] = 1 + Ksv[Q] \quad (4)$$

where [Q] is the added concentration of CPs; F_0 and F denote the fluorescence intensity of the composite system without and with the introduction of CPs, respectively. K_q represents the rate constant in the quenching process, K_{sv} is the Stern-Volmer quenching constant, and τ_0 is the average lifetime of fluorescent molecules without the presence of CPs ($\tau_0 = 10^{-8}$ s).

Dynamic quenching is typically due to the collision between the fluorescent agent and the quencher, while static quenching is the result of the formation of a stable fluorescent agent-quencher complex (Sadeghi-kaji, Shareghi, Saboury, & Farhadian, 2019). Dynamic quenching is characterized by the fact that the quenching constant increases with increasing temperature, as the latter promotes intermolecular collisions. However, in static quenching, the quenching constant decreases with increasing temperature (Acharya, Sanguansri, & Augustin, 2013).

Therefore, the influence of temperature on the interaction between CG and CPs was investigated and fitted using Eq. (4) to obtain K_{sv} and K_q. As shown in Table 1, the K_{sv} for all CG-CPs decreased with increasing temperature. The K_{sv} for CHA-CG was highest at 298, 303, and 308 K, suggesting that CG has the greatest influence on CHA molecules. Furthermore, the minimum quenching rate constant K_q was 4.07×10^{12} L·mol^{-1}·s^{-1}, which was significantly higher than the maximum dynamic quenching constant (2.0×10^{10} mol^{-1}·s^{-1}) (Sadeghi-kaji et al., 2019). These results further confirmed that the fluorescence quenching mechanism of CPs on CG was static quenching caused by nonradiative energy transfer from the complexes formed between CG and CPs.

Static quenching was used to calculate the binding constant (K_a) of the complexes between CG and CPs and the number of binding sites (n) of the protein. This can be achieved using the following logarithmic Eq. (5) (Tian et al., 2023):

$$\log\frac{F0 - F}{F} = \log Ka + n\log[Q]\log\frac{F0 - F}{F} = \log Ka + n\log[Q] \quad (5)$$

The values of K_a and n indicated the binding capacity of CPs to CG. Higher K_a and n values meant a stronger interaction between the protein and CPs, indicating more stable complex formation. All K_a values were well above 10^4 L·mol^{-1}, indicating that CG and CPs had strong binding affinity. The K_a values for CG-CA and CG-CHA decreased with increasing temperature, suggesting that the interaction between CG and CA/CHA was less favorable at higher temperatures. Conversely, higher temperatures promoted the interaction between CG and FA.

These results are consistent with those of Qi et al. (2023) where it was found that when trypsin bound to CA and CHA, the K_a of trypsin-CA was lower than that of trypsin-CHA. The increased binding affinity could be due to the presence of a larger number of hydroxyl groups in CHA, which facilitated the formation of hydrogen bonds with proteins, thus leading to a more robust interaction. At 298 K, both K_a and n values for CG-CHA were larger than those of CG-CA and CG-FA, indicating the strongest combination between CHA and CG (Tian et al., 2023). The n values for CG-CPs were greater than 1, suggesting that CA/CHA/FA and CG had an additional binding site.

To further identify the main driving forces (hydrogen bonds, hydrophobic forces, and electrostatic forces) behind the interaction of CG and CPs, thermodynamic parameters were calculated using Van't Hoff Eqs. (6) and (7) (Tian et al., 2023):

$$\ln Ka = -\frac{\Delta H}{RT} + \frac{\Delta S}{R} \quad (6)$$

$$\Delta G = \Delta H - T\Delta S \quad (7)$$

here, T denotes the absolute temperature; R represents the gas constant, which is 8.314 J·mol^{-1}·K^{-1}; ΔH, ΔS, and ΔG represent changes in enthalpy, entropy, and Gibbs free energy, respectively.

The thermodynamic parameters ΔH and ΔS provide insights into the dominant forces in a given interaction. When $\Delta H > 0$ and $\Delta S > 0$, hydrophobic forces predominate. If $\Delta H < 0$ and $\Delta S < 0$, this suggests that van der Waals forces or hydrogen bonds dominate. If $\Delta H < 0$ and $\Delta S > 0$, it means that electrostatic interactions are the main factor (Liu et al., 2020). According to Table 1, ΔH and ΔS values of CG-CA and CG-CHA were below 0, indicating that the interaction between CA/CHA and CG was predominantly driven by hydrogen bonds and van der Waals

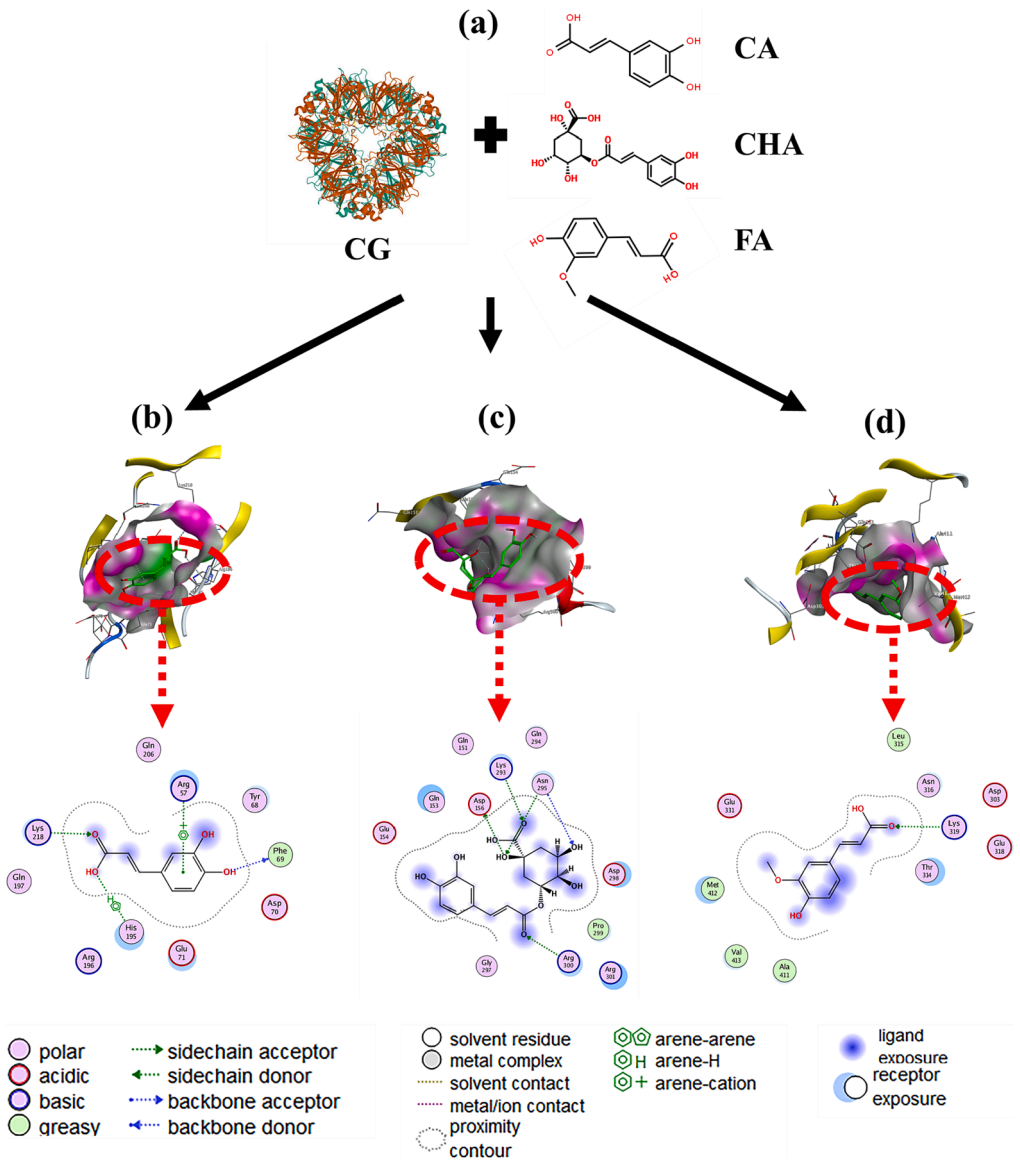

Fig. 2. Molecular docking of CG with CA, CHA, and FA. Crystal structure of CG and structural formula for CA, CHA, and FA (a); The whole stimulated 3D docking mode and schematic diagram of the interaction between 2D docking amino acid residues of CG-CA (b), CG-CHA (c), and CG-FA (d).

forces. These results were consistent with the study showing that these forces were the main drivers in the interaction between CA/CHA and trypsin (Qi et al., 2023). However, other research found that the whey protein-CHA complex was mainly stabilized through hydrophobic interaction (Zhang et al., 2021). These variations could be attributable to differences in protein type and solvent pH. Moreover, ΔH and ΔS values of CG-FA were below 0, suggesting that hydrophobic forces dominated in the interaction between FA and CG. All ΔG values were less than 0, suggesting that the reactions between CG and CA/CHA/FA were spontaneous (Zhang et al., 2021).

Protein fluorescence originated from aromatic amino acid residues, mainly tryptophan (Trp). Consequently, the endogenous fluorescence spectrum could highlight changes in the spatial structure of proteins caused by the interaction between polyphenols and proteins (Parolia et al., 2022). With the increase in CA, CHA, and FA concentrations, the fluorescence intensity of CG continuously decreased. Additionally, at 298 K and a concentration of CA, CHA, and FA of 140 μmol/L, there was an obvious red shift of the maximum fluorescence intensity from CG (336 nm) to 353 nm for CG-CA, 368 nm for CG-CHA, and 350 nm for CG-FA. This shift signified that the molecular structure of CG unfolded due to the interaction with CPs and the internal Trp residues of CG were exposed to a polar environment (Qi et al., 2023).

Molecular docking technology can provide deeper insights into the interaction between CPs and CG by visualizing the binding sites and interaction forces between receptor and ligand molecules (Chen et al., 2023b). Fig. 2 displays the 3D docking mode and the interaction between two-dimensional docking amino acid residues of a docking simulation. The order of molecular docking energy between CG and CPs was CG-CHA (-6.01 kJ/mol) < CG-FA (-5.34 kJ/mol) < CG-CA (-4.36 kJ/mol), indicating that the CG-CHA complex had the most stable molecular conformation. This finding was consistent with those of fluorescence fitting. The hydrogen bond interaction between CG and CA was mediated by Lys 218, His 195, and Arg 57. CG and CHA interacted through four hydrogen bonds involving the amino acids His 156, Lys 293, Arg 295, and Asn 300. A hydrogen bonding interaction was found between CG and FA via Lys 319. These results highlighted that the primary driving force for the formation of the CG-CPs complex was mainly hydrogen bonds.

In conclusion, all CPs could interact robustly with CG. Due to the limited –OH and –COOH groups, the interaction between CG and FA was

primarily hydrophobic, followed by hydrogen bonding. CA had two –OH groups and one –COOH group, ensuring that its noncovalent interactions with CG molecules were dominated by hydrogen bonds, followed by hydrophobic interactions (Qi et al., 2023). CHA was composed of esters formed by CA and quinic acid (Mortele et al., 2021), suggesting that CHA could easily form noncovalent interactions with the protein. As expected, CHA formed a stable complex with CG through strong hydrogen bonds and hydrophobic interactions.

Effect of CPs on CG structure

Fig. S1**a** shows the SDS-PAGE results of CG, CG-CA, CG-CHA, and CG-FA. In their reduced forms, CG and CG-CPs were observed to be between 17 and 55 kDa. Predominantly, CG and CG-CPs exhibited a 55 kDa band that corresponds to 11S globulin (cocosin), which played a vital role in maintaining the stability of coconut milk (Patil & Benjakul, 2017). In its native state, 11S globulin exists as a hexamer and consists primarily of two acidic polypeptides (32 kDa) and two basic polypeptides (22 kDa), which are linked via disulfide bonds (Carr, Plumb, & Lambert, 1990). Furthermore, 7S globulin, another key protein, consists of bands at 19, 29, and 33 kDa (Benito, Gonzalez-Mancebo, de Durana, Tolon, & Fernandez-Rivas, 2007). As shown in Fig. S1**a**, the bands of the CG-CPs complexes mirrored those of CG with no new bands evident, indicating that the CG-CPs complexes were formed through noncovalent interactions rather than the formation of one new substance via covalent bonding (Ma et al., 2023). Due to the incorporation of CA, CHA, and FA, the 55 kDa band demonstrated slightly deeper staining. At the same time, the bands corresponding to lower molecular weight components of CG-CPs gradually faded. These observations suggested the formation of macromolecular aggregated as a result of the interaction between CG and CPs.

The interaction between CPs and CG could indeed actually lead to rearrangement of the intermolecular forces that maintain the secondary structure of CG, leading to conformational changes in CG. Far-UV CD analysis is widely used to investigate such changes in secondary structure upon binding with CPs. As illustrated in Fig. S1**b**, the main chain conformation of CG in the 190–250 nm range showed two negative peaks at 208 and 222 nm. This is a typical feature of the protein α-helix structure. These two negative peaks at 208 nm and 220 nm generally represent the π-π * and n-π* transitions of α-helix peptide bonds (Chen et al., 2023c), respectively. The addition of CA, CHA, and FA resulted in a reduction in the molar ellipticity of these negative peaks, indicating a reduction in the α-helix of CG due to its partial unfolding and destabilization (Zhang, Sahu, Xu, Wang, & Hu, 2017). CPs had the potential to interact with the side chains of various amino acid residues in CG and the carbonyl and amino groups in peptide bonds, leading to the formation of hydrogen bonds. Such interactions could alter the hydrogen bond structure and loosen the peptide chain in the native protein, leading to denaturation of the protein. Therefore, the interaction between CG and CPs disrupted the secondary structure of CG molecules and converted them from a loosely structured order-dominated form to a partially disordered structure.

FTIR spectroscopy is indeed an excellent tool for understanding the functional groups involved in the binding between CG and CPs. The FTIR spectra of CG exhibit a robust and broad absorption peak at 3303 cm^{-1}, which is attributed to O—H and N—H stretching vibrations. This signified the formation of hydrogen bonds (Liu et al., 2022). When CG was combined with CA, CHA, and FA, the peak of CG shifts from 3303 cm^{-1} to 3423 cm^{-1}, 3436 cm^{-1}, and 3421 cm^{-1} (Fig. S1**c**), respectively. This shift could be related to the hydrogen bond interaction between CG and CA/CHA/FA. The expansion of the CG molecular structure facilitated by the addition of CPs provided more binding sites for hydrogen bonds, thereby promoting the formation of these bonds. However, the strength of the hydrogen bonds was influenced by the type of CPs. CHA, with more –OH and –COOH groups, showed the most obvious red-shift, indicating a stronger interaction. In addition, the FTIR spectra of CG at the absorption peak of 2926 cm^{-1}, which corresponds to the C—H tensile vibration of methyl and methylene, can be used to characterize the hydrophobic interaction between CG and CPs. All CG-CPs complexes exhibited a blue shift at this peak, indicating the presence of hydrophobic interactions (Wang et al., 2022). Lastly, the characteristic absorption peaks of the amide I region (1600–1700 cm^{-1}) and amide II region (1500–1600 cm^{-1}) in the FTIR spectra represent significant structural features of proteins. The amide I region is caused by the stretching vibration of C═O and the bending vibration of N—H, while the amide II region is caused by the stretching vibration of C—N and the bending vibration of N—H (Chen et al., 2023c). Upon interaction with CPs, changes in the amide I band of CG indicated changes in the CG structure due to the formation of the complex.

Indeed, changes in the amount of free -SH groups and S—S bonds in proteins can provide valuable insights into the structural transformations of these proteins. Free -SH groups in CG-CA and CG-CHA were observed to decrease significantly, while no significant change was observed for CG-FA ($p < 0.05$) (Fig. S1**d**). Moreover, the content of S—S bonds increased in CG-CA and CG-CHA. This phenomenon could be attributed to the strong reactivity of the –OH groups of CPs, which interacted with the free -SH groups of CG, thereby reducing the presence of free -SH groups.

In summary, the presence of CPs led to the formation of macromolecular aggregates with CG. The interaction between CPs and CG promoted the structural transformation of proteins from an ordered structure to a disordered one. This expansion of the protein structure provided more sites for CPs to form hydrogen bonds. However, it was worth noting that the structural influence of CPs on CG depended on the type of CPs, and the order in terms of impact was CHA > CA > FA. This observation correlated with the strength of hydrogen bond formation, with the bond between CHA and CG being the strongest.

Effect of CPs on particle size, polymer dispersion index (PDI), zeta potential, and turbidity of CG

Fig. S2 illustrates the particle size, PDI, zeta potential, and turbidity of CG and CG-CPs. In Fig. S2**a**, the average particle size of CG was found to be 228 nm, and the PDI was 0.35. With the addition of CPs, the particle sizes of CG-CA, CG-CHA, and CG-FA significantly increased to 247, 245, and 249 nm, respectively ($p < 0.05$), signifying that CPs caused CG aggregation. These findings results were consistent the study of Feng et al. (2021) that found that the average particle size and zeta potential of nanoparticles can be controlled through interactions with pectin and soy protein isolate. The TEM images further confirmed that the interaction between CG and CPs resulted in an increase in CG particle size, as shown in Fig. S2**b**. Conversely, the PDI values of CG-CA, CG-CHA, and CG-FA decreased to less than 0.35, suggesting that the presence of CPs contribute to achieve a more uniform dispersion within the system. Additionally, the absolute potential values for CG, CG-CA, and CG-CHA complexes were found to be higher than that of CG (-12.07 mV). These data implied that CPs facilitated CG to expose more negatively charged amino acid residues, thereby enhancing electrostatic repulsion between complex molecules and inhibiting their aggregation. Compared to CG, the turbidity values of CG-CA, CG-CHA, and CG-FA were increased, with CG-CHA showing a significant increase ($p < 0.05$). This increase could be attributed to the interactions between CG and CA/CHA/FA.

In conclusion, the interactions between CG and CPs led to an increase in both particle size and absolute potential value, while the PDI of CG-CPs decreased. These changes signified an enhancement in the stability of CG-CPs complexes, reflecting the critical role of CPs in modulating the physical properties of the system.

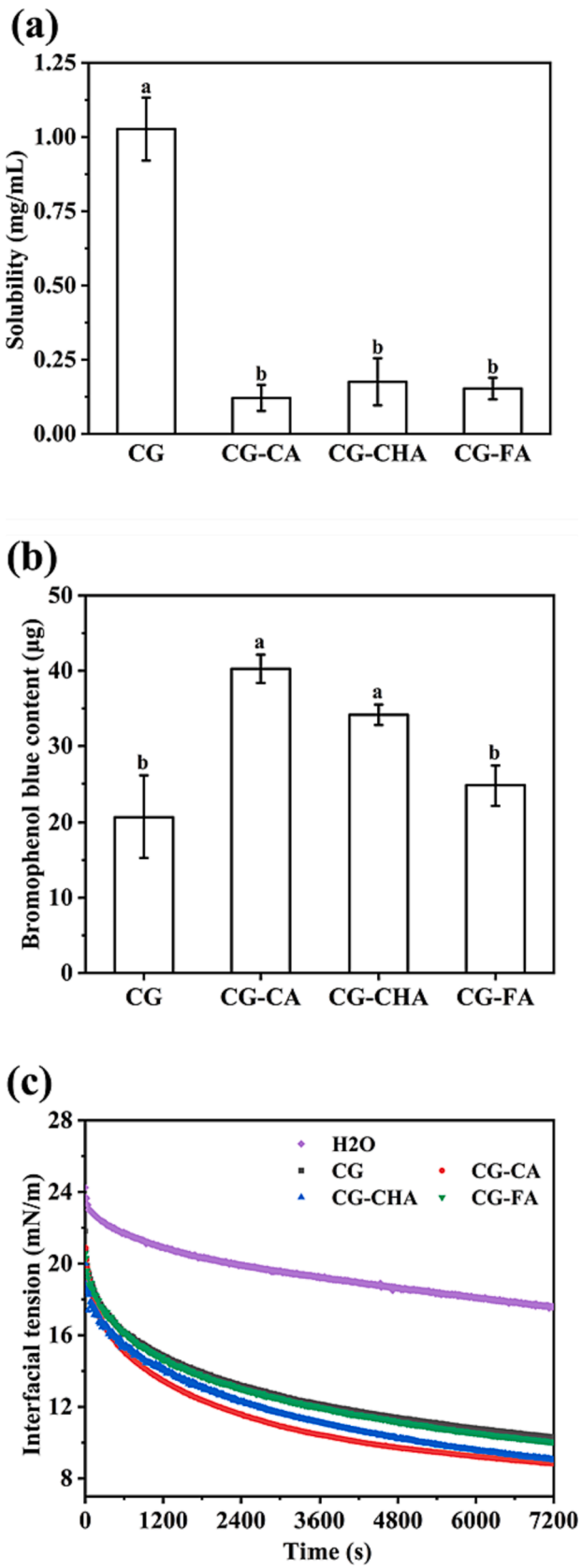

Fig. 3. Solubility (a), surface hydrophobicity (b), and dynamic interfacial tension of protein adsorption at O/W interface (c). Different lowercase letters indicated significant differences between samples ($p < 0.05$).

Effect of CPs on solubility, surface hydrophobicity, and interfacial tension of CG

For the successful integration of proteins into various food systems, a comprehensive understanding of their functional properties is essential, as these properties may exhibit different behaviors in different food contexts. Specifically, the solubility, surface hydrophobicity, and interfacial properties of proteins play a crucial role in determining their emulsifying ability (Bertsch, Mayburd, & Kassner, 2003). Given this background, the present study conducted a detailed characterization of CG and CG-CPs, focusing on these critical aspects to shed light on their potential applications and behavior in different food environments.

As illustrated in Fig. 3**a**, the solubility of CG noticeably diminished in the presence of CPs. The –OH and –COOH groups of CA, CHA, and FA acted as powerful hydrogen bond donors and acceptors, forming robust hydrogen bonds with the peptide backbone. Owing to the relatively low molecular weights of CA, CHA, and FA, a single CG molecule could interact with multiple CA/CHA/FA molecules (as evidenced by the results of molecular docking simulations). This intervention led to the formation of a network with an interconnected structure, subsequently causing precipitation. Furthermore, the CG structure was extended by CPs, exposing the internal hydrophobic groups. This exposure hindered the interaction between the hydrophilic groups on the surface of protein and water molecules, further contributing to the observed decrease in solubility.

Fig. 3**b** shows the surface hydrophobicity results of CG, CG-CA, CG-CHA, and CG-FA. For proteins with low solubility, the bromophenol blue method proves to be more suitable than the fluorescence probe method using 8-anilinonaphthalene-1-sulfonic acid. The amount of bound bromophenol blue serves as an indicator of surface hydrophobicity; the higher the content, the more pronounced the hydrophobicity (Bertsch et al., 2003). In its native state, CG exhibited relatively weak surface hydrophobicity. This could be attributed to the abundance of hydrophilic groups on the CG surface, while the hydrophobic groups were predominantly located in the interior (Tangsuphoom & Coupland, 2009). The addition of CPs facilitated the unfolding of the CG molecular structure, thereby exposing the internal hydrophobic groups, which subsequently led to an enhancement in hydrophobicity.

During the formation of the O/W interfacial film, the hydrophobic groups of the protein orient toward the oil phase while the hydrophilic groups point to the water phase, which helps to reduce the interfacial tension between the water and oil phases. The hydrophobic groups of the CG molecules were gradually adsorbed on the surface of the oil droplets and then rearranged to form an interfacial film (Liao, Elaissari, Dumas, & Gharsallaoui, 2023). Compared to the equilibrium interfacial tension of water (17.57 mN/m), the interfacial tensions of CG, CG-CA, CG-CHA, and CG-FA were significantly reduced to 10.32, 8.83, 9.02, and 10.05 mN/m, respectively. As a globular protein, CG exhibited a low rearrangement rate since it maintained its original conformation at the O/W interface (Han, Liu, & Tang, 2023). As illustrated in Fig. 3**c**, after adsorption and rearrangement, CG formed a thin interfacial film at the O/W interface, an effect attributed to its poor surface hydrophobicity. The polyphenols CA, CHA, and FA promoted the unfolding of CG, thereby exposing more hydrophobic groups and enhancing the protein-oil interaction. The noncovalent interactions between FA and CG were predominantly hydrophobic, exerting a moderate influence on the structure of CG. Conversely, the –COOH and –OH groups of CA could form hydrogen bonds with the amino acid residues of CG, fostering the formation of a dense and thick interfacial film at the O/W interface. Notably, the presence of quinic acid in CHA molecules introduced additional hydrogen bonding groups that interacted with CG. This caused CG-CHA molecules being more prone to form a robust and substantial interfacial film at the O/W interface. In summary, the hydrogen bonds between CG and CPs promoted molecular cross-linking at the O/W interface, resulting in a dense and thick interfacial film. Additionally, CPs facilitated the formation of S—S, which further increased the

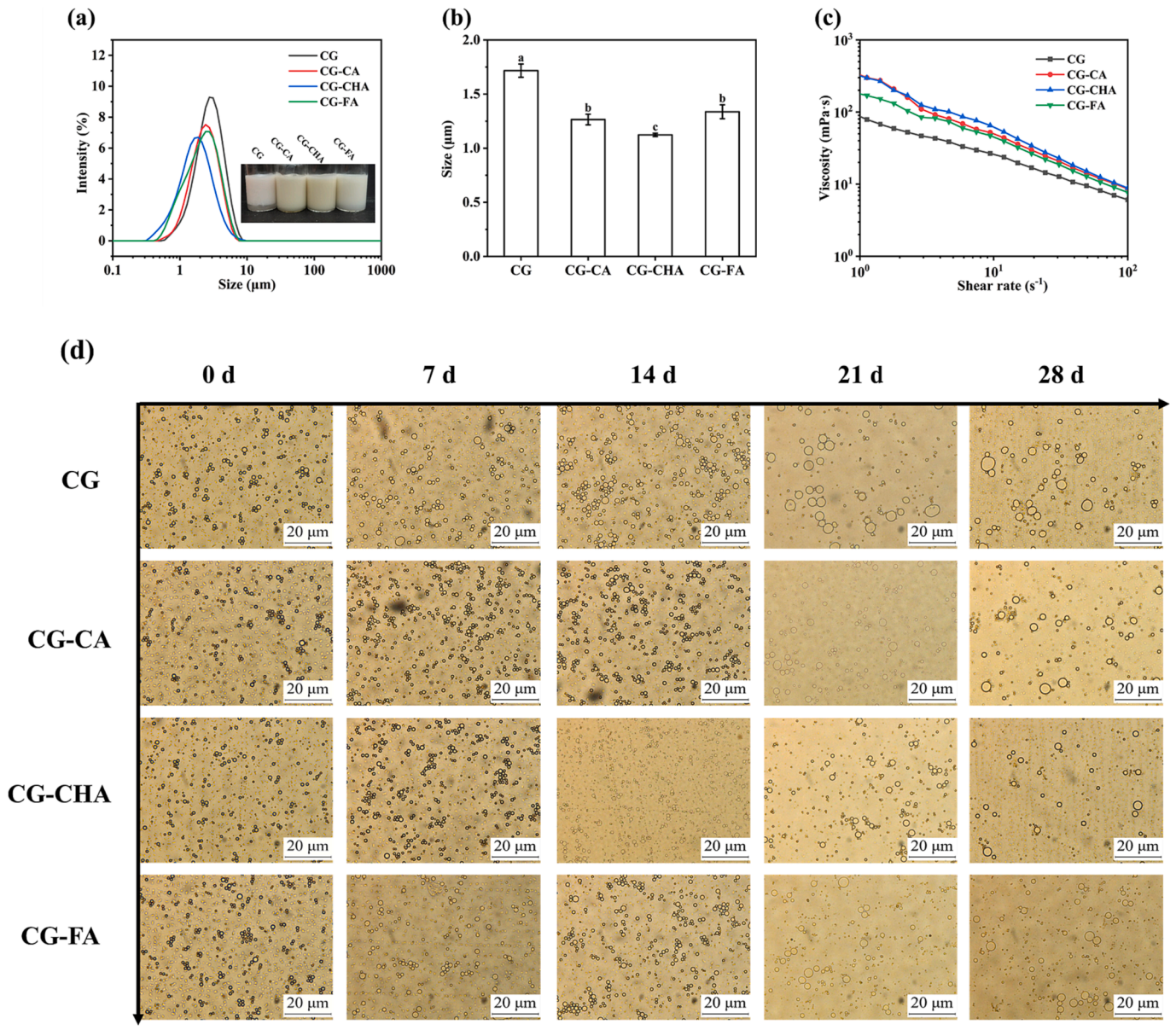

Fig. 4. Droplet size distribution (a), droplet size (b), and viscosity (c) of the emulsion stabilized by CG, CG-CA, CG-CHA, and CG-FA; The corresponding photomicrographs (d) of the emulsion stabilized by CG, CG-CA, CG-CHA, and CG-FA after storing. Different lowercase letters indicated significant differences between samples ($p < 0.05$).

stability and viscoelasticity of the interfacial film.

The interaction between CPs and CG promoted the unfolding of the structure of CG, leading to a masking of surface hydrophilic groups and a subsequent decrease in interaction with water molecules, as evidenced by the reduced solubility. Concurrently, this interaction facilitated the exposure of internal hydrophobic groups, resulting in an increase in surface hydrophobicity. These noncovalent interactions between CG and CPs caused the peptide chain to extend and expose the aromatic amino acids in the protein. Consequently, the affinity of CG-CPs to the O/W interface was enhanced. Particularly noteworthy was the robust hydrogen bonds between CHA and CG, which proved beneficial for the formation of a dense and thick interfacial membrane at the O/W interface. The adsorption mechanism diagram of CG, CG-CA, CG-CHA, and CG-FA at the O/W interface is shown in Fig. S3.

Physical properties of emulsion stabilized by CG and CG-CPs

Fig. 4**a-b** illustrate the droplet sizes of emulsions stabilized by CG, CG-CA, CG-CHA, and CG-FA. The droplet sizes of emulsions stabilized by CG-CPs were found to be smaller than those stabilized by free CG at 1.72 μm. This observation demonstrated that droplet aggregation was effectively inhibited in CG-CPs stabilized emulsions. This inhibition could be due to an increase in electrostatic repulsion and steric hindrance between droplets, especially for CHA. Fig. 4**c** presents the apparent viscosity of the emulsions stabilized by CG and CG-CPs. The apparent viscosity of these emulsions decreased with increasing shear rate, indicating that the emulsions were either destroyed or dissolved during shear (Chen et al., 2023a). This interaction between CG and CPs appeared to promote the cross-linking of the droplets, leading to an increase in the apparent viscosity. The phenomenon suggested that the interaction between CG and CPs restricted the movement of molecules due to the formation of a convoluted cross-linking structure. Moreover, a strong hydrogen bonding interaction between CG and CHA led to extensive cross-linking and a denser structure, which in turn resulted in an increase in viscosity. Additionally, CG-CPs exhibited greater deformation resistance at the O/W interface, which was likely due to the

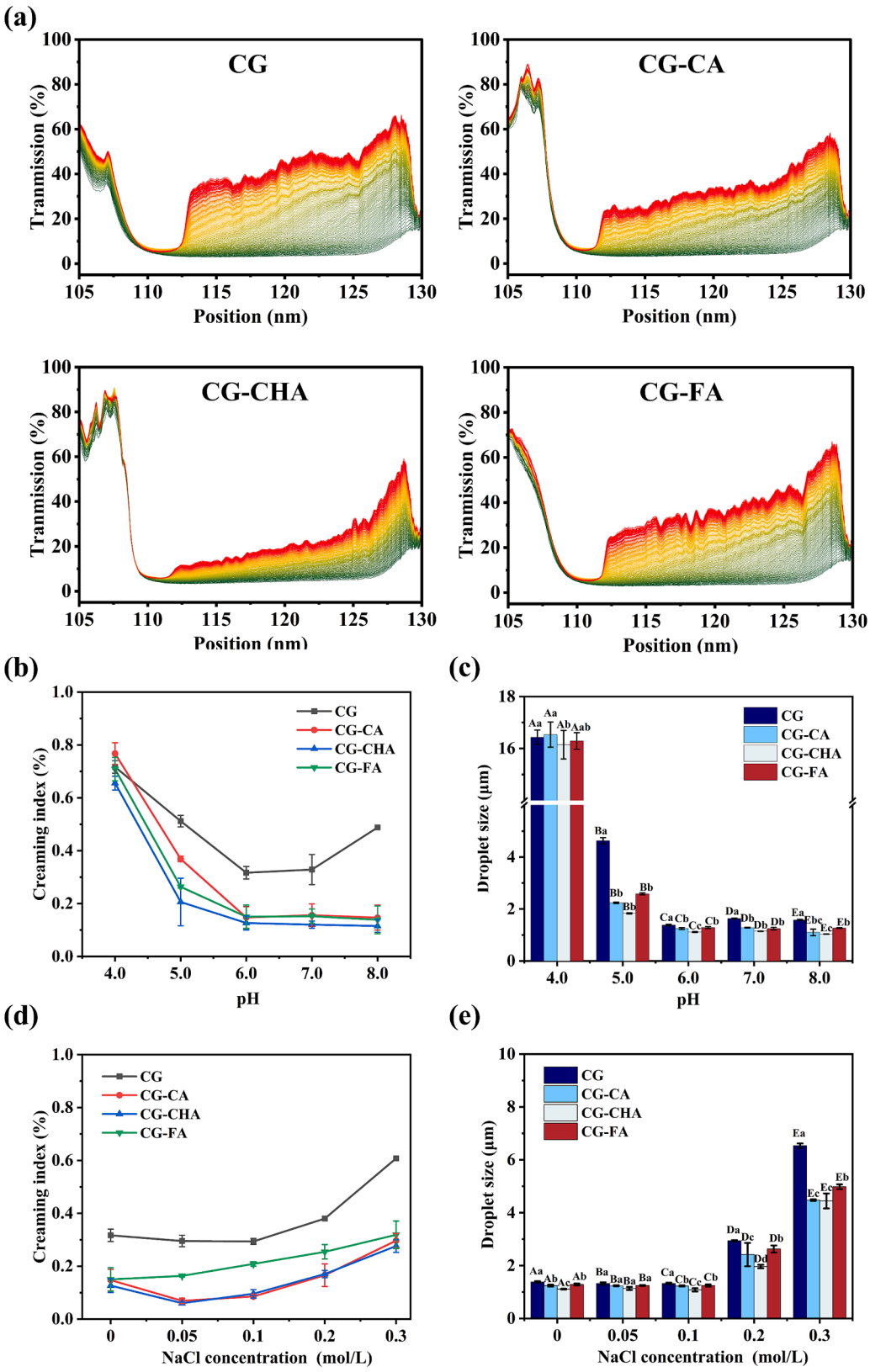

Fig. 5. Spectrum of stability analysis of the emulsion stabilized by CG, CG-CA, CG-CHA, and CG-FA composite. Profiles started at the red line and end to the green line (a); Creaming index (b), and droplet size (c) of the emulsion stabilized by CG, CG-CA, CG-CHA, and CG-FA composite at different pH. Creaming index (d), and droplet size (e) of the emulsion stabilized by CG, CG-CA, CG-CHA, and CG-FA after adding various concentration of NaCl. Different capital and lowercase letters indicated significant differences between samples ($p < 0.05$). (For interpretation of the references to colour in this figure legend, the reader is referred to the web version of this article.)

formation of a dense and thick interfacial film.

Storage stability, centrifugal stability, pH stability, and salt stability of emulsion stabilized by CG and CG-CPs

In order to demonstrate the effect of noncovalent interactions between CG and CPs on the storage stability of the emulsion, the changes in the droplet microstructure of the emulsion were recorded over a period of 28 days (Fig. 4**d**). Within the CG-stabilized emulsion, droplets were observed to merge and aggregate. Conversely, the fresh emulsion droplets stabilized by CG-CPs were small and uniform in size. In all instances, the droplet size in the emulsion gradually increased with the extension of the storage time, highlighting that the emulsion became unstable during storage. This instability could be due to the flocculation and coalescence of the emulsion droplets (Liu, Xu, Xia, & Jiang, 2021). After 28 days of storage, the coalesced oil droplets were more prominent in the CG-stabilized emulsion, while the emulsion stabilized by CG-CPs experienced slight changes. These findings confirmed that the emulsions stabilized by CG-CPs were relatively more stable, especially those stabilized by CG-CHA.

In this study, when the emulsion was irradiated with parallel near-infrared light, the temporal and spatial changes in the transmitted light through the liquid over time and space during centrifugation were recorded, as shown in the transmission curve. After centrifugation, the emulsion became unstable, with the heavier water phase settling to the bottom of the cuvette and the lighter oil droplets migrating to the top. Consequently, the movement of the emulsion droplets was visualized by the intensity of transmitted light over time, allowing quantification of the unstable process within the emulsion droplets (Chen et. al., 2023c). Fig. 5**a** depicts the change in light transmittance of CG and CG-CPs stabilized emulsions during centrifugation. The CG-stabilized emulsion stabilized exhibited a rapid shift in light transmittance, with the transmittance of most emulsions increasing from less than 10 % to over 40 %. This indicated that it quickly became unstable during centrifugation. In contrast, the emulsions stabilized by CG-CPs effectively improved the centrifugal stability, showing a gradual increase in light transmittance. Notably, after the centrifugation of the CG-CHA-stabilized emulsion, most emulsion layers maintained a light transmittance below 20 %, suggesting a higher degree of stability.

Fig. S4 and Fig. 5**b-c** demonstrate the effects of pH on the visual appearance, CI, and droplet size of the prepared emulsion. Between pH values of 6.0 and 8.0, the emulsions stabilized by CG and CG-CPs remained relatively stable, showing slight changes in droplet size. However, when the pH value decreased to 4.0, the droplet size of emulsions stabilized by CG and CG-CPs increased to about 16 μm. This indicated that droplets aggregated into larger units near the isoelectric point (pI ≈ 4.3). CG, being an acidic protein, typically had a relatively low surface charge in an acidic environment (pH 4.0–5.0) and was prone to aggregation, leading to decreased emulsion stability (Chen et. al., 2023). At pH values of 4.0 and 5.0, the emulsions stabilized by CG, CG-CA, and CG-FA separated into a transparent serum layer at the bottom of the container, while the emulsion stabilized by CG-CHA showed no detectable phase separation. When the pH was neutral or alkaline, CA, CHA, and FA were prone to oxidation, especially CA and CHA, which had a catechol structure and can oxidize to quinone. This structure could react with nucleophilic groups in CG and covalently couple to form yellow polymers. Additionally, the covalent coupling of CG with CA/CHA/FA could promote further protein development and exposure of hydrophobic groups, enhancing emulsifying properties (Lin et al., 2022).

Fig. S5 and Fig. 5**d-e** present a study on the effects of varying salt ion concentrations on the stability of emulsions stabilized by CG and CG-CPs, based on visible appearance, CI, and droplet size. At low Na^+ concentrations (0–0.1 mol/L), the emulsifying stability of the emulsion improved due to the salt dissolution effect. However, after adding 0.2–0.3 mol/L NaCl solution, the electrostatic repulsion between droplets was masked by salt ions, leading to droplet aggregation and coalescence (Yu, Wang, Li, & Wang, 2022). Both the droplet size and CI of emulsions stabilized by CG-CPs were significantly smaller than those of CG-stabilized emulsions. These results indicated that CG-CPs complexes effectively enhanced the salt ion stability of the emulsion after modification with CPs.

Conclusion

In this study, CA, CHA, and FA were selected as representative polyphenols of CPs to investigate the underlying mechanism by which CPs enhance the emulsification stability of CG. It was found that the interactions among CA, CHA, and CG were mainly characterized by hydrogen bonds, with CHA being particularly notable in this regard. This was attributed to the inclusion of quinic acid in CHA, which provided additional –OH and –COOH groups, thereby leading to the strongest hydrogen bonding with CG. Furthermore, the interactions between FA and CG were mainly controlled by hydrophobic forces. These specific interactions caused the protein structure of CG to unfold and expose the hydrophobic groups, thereby promoting the formation of a dense and robust interfacial film at the O/W interface. As a result, the emulsions stabilized by CG-CPs exhibited remarkable stability across various measures such as storage, centrifugation, pH values, and salt tolerance, with the emulsions stabilized by CG-CHA being particularly effective. This study thus provides a solid theoretical basis for improving the stability of CG and coconut milk and offers innovative insights into the potential applications of coconut milk in the food industry.

Declaration of Competing Interest

The authors declare that they have no known competing financial interests or personal relationships that could have appeared to influence the work reported in this paper.

Data availability

Data will be made available on request.

Acknowledgments

The authors gratefully acknowledge the financial support from the Science and Technology Plan Project of Haikou (No. 2022-014), the Research Project of the Collaborative Innovation Center of Hainan University (No. XTCX2022NYB13), and the Innovation Platform for Academicians of Hainan Province.

Appendix A. Supplementary data

Supplementary data to this article can be found online at https://doi.org/10.1016/j.fochx.2023.100954.

References

Acharya, D. P., Sanguansri, L., & Augustin, M. A. (2013). Binding of resveratrol with sodium caseinate in aqueous solutions. *Food Chemistry, 141*(2), 1050–1054. https://doi.org/10.1016/j.foodchem.2013.03.037

Ariyaprakai, S., Limpachoti, T., & Pradipasena, P. (2013). Interfacial and emulsifying properties of sucrose ester in coconut milk emulsions in comparison with Tween. *Food Hydrocolloids, 30*(1), 358–367. https://doi.org/10.1016/j.foodhyd.2012.06.003

Arlai, A., & Tananuwong, K. (2021). Quality of chilled and frozen starch gels as affected by starch type, highly concentrated sucrose and coconut milk. *LWT - Food Science and Technology, 147*, Article 111534. https://doi.org/10.1016/j.lwt.2021.111534

Benito, C., Gonzalez-Mancebo, E., de Durana, M. D. A. D., Tolon, R. M., & Fernandez-Rivas, M. (2007). Identification of a 7S globulin as a novel coconut allergen. *Annals of Allergy, Asthma & Immunology, 98*(6), 580–584. https://doi.org/10.1016/s1081-1206(10)60739-9

Bertsch, M., Mayburd, A. L., & Kassner, R. J. (2003). The identification of hydrophobic sites on the surface of proteins using absorption difference spectroscopy of

bromophenol blue. *Analytical Biochemistry, 313*(2), 187–195. https://doi.org/10.1016/s0003-2697(02)00590-0

Bondam, A. F., da Silveira, D. D., dos Santos, J. P., & Hoffmann, J. F. (2022). Phenolic compounds from coffee by-products: Extraction and application in the food and pharmaceutical industries. *Trends in Food Science & Technology, 123*, 172–186. https://doi.org/10.1016/j.tifs.2022.03.013

Carr, H. J., Plumb, G. W., & Lambert, M. L. P. N. (1990). Characterisation and crystallisation of an 11S seed storage globulin from coconut (Cocos nucifera). *Food Chemistry, 38*, 11–20. https://doi.org/10.1016/0308-8146(90)90202-F

Chelh, I., Gatellier, P., & Sante-Lhoutellier, V. (2006). Technical note: A simplified procedure for myofibril hydrophobicity determination. *Meat Science, 74*(4), 681–683. https://doi.org/10.1016/j.meatsci.2006.05.019

Chen, Y., Chen, Y. L., Fang, Y. J., Pei, Z. S., & Zhang, W. M. (2024). Coconut milk treated by atmospheric cold plasma: Effect on quality and stability. *Food Chemistry, 430*, Article 137045. https://doi.org/10.1016/j.foodchem.2023.137045

Chen, Y., Chen, Y. L., Jiang, L. Z., Yang, Z. H., Fang, Y. J., & Zhang, W. M. (2023a). Shear emulsification condition strategy impact high internal phase Pickering emulsions stabilized by coconut globulin-tannic acid: Structure of protein at the oil-water interface. *LWT - Food Science and Technology, 187*, Article 115283. https://doi.org/10.1016/j.lwt.2023.115283

Chen, Y., Yao, M. Y., Peng, S., Fang, Y. J., Wan, L. T., Shang, W. T., et al. (2023b). Development of protein-polyphenol particles to stabilize high internal phase Pickering emulsions by polyphenols' structure. *Food Chemistry, 428*, Article 136773. https://doi.org/10.1016/j.foodchem.2023.136773

Chen, Y., Yao, M. Y., Yang, T. Y., Fang, Y. J., Xiang, D., & Zhang, W. M. (2023c). Changes in structure and emulsifying properties of coconut globulin after the atmospheric pressure cold plasma treatment. *Food Hydrocolloids, 136*, Article 108289. https://doi.org/10.1016/j.foodhyd.2022.108289

Condict, L., & Kasapis, S. (2022). Critical issues encountered in the analysis of protein-phenolic binding interactions via fluorescence spectroscopy. *Food Hydrocolloids, 124*, Article 107219. https://doi.org/10.1016/j.foodhyd.2021.107219

Feng, S. M., Yan, J. D., Wang, D., Jiang, L. G., Sun, P. L., Xiang, N., et al. (2021). Preparation and characterization of soybean protein isolate/pectin-based phytosterol nanodispersions and their stability in simulated digestion. *Food Research International, 143*, Article 110237. https://doi.org/10.1016/j.foodres.2021.110237

Han, W., Liu, T. X., & Tang, C. H. (2023). Transforming monomeric globulins into pickering particles to stabilize nanoemulsions: Contribution of trehalose. *Food Hydrocolloids, 141*, Article 108687. https://doi.org/10.1016/j.foodhyd.2023.108687

Kwon, K., Park, K. H., & Rhee, K. C. (1996). Fractionation and characterization of proteins from coconut (Cocos nucifera L.). *Journal of Agricultural and Food Chemistry, 44*, 1741–1745. https://doi.org/10.1021/JF9504273

Li, Y. T., He, D., Li, B., Lund, M. N., Xing, Y. F., Wang, Y., et al. (2021). Engineering polyphenols with biological functions via polyphenol-protein interactions as additives for functional foods. *Trends in Food Science & Technology, 110*, 470–482. https://doi.org/10.1016/j.tifs.2021.02.009

Liao, W., Elaissari, A., Dumas, E., & Gharsallaoui, A. (2023). Effect of trans-cinnamaldehyde or citral on sodium caseinate: Interfacial rheology and fluorescence quenching properties. *Food Chemistry, 400*, Article 134044. https://doi.org/10.1016/j.foodchem.2022.134044

Lin, X., Ye, L. Y., He, K., Zhang, T. T., Sun, F., Mei, T. T., et al. (2022). A new method to reduce allergenicity by improving the functional properties of soybean 7S protein through covalent modification with polyphenols. *Food Chemistry, 373*, Article 131589. https://doi.org/10.1016/j.foodchem.2021.131589

Liu, C. K., Xu, Y. S., Xia, W. S., & Jiang, Q. X. (2021). Enhancement of storage stability of surimi particles stabilized novel pickering emulsions: Effect of different sequential ultrasonic processes. *Ultrasonics Sonochemistry, 79*, Article 105802. https://doi.org/10.1016/j.ultsonch.2021.105802

Liu, J. Y., Song, G. S., Yuan, Y. W., Zhou, L. K., Wang, D. L., Yuan, T. L., et al. (2022). Ultrasound-assisted assembly of beta-lactoglobulin and chlorogenic acid for non covalent nanocomplex: Fabrication, characterization and potential biological function. *Ultrasonics Sonochemistry, 86*, Article 106025. https://doi.org/10.1016/j.ultsonch.2022.106025

Liu, Y. X., Huang, L., Li, D. H., Wang, Y. B., Chen, Z. H., Zou, C., et al. (2020). Re-assembled oleic acid-protein complexes as nano-vehicles for astaxanthin: Multispectral analysis and molecular docking. *Food Hydrocolloids, 103*, Article 105689. https://doi.org/10.1016/j.foodhyd.2020.105689

Lu, Y. C., Zhao, R., Wang, C., Zhang, X. G., & Wang, C. N. (2022). Deciphering the non-covalent binding patterns of three whey proteins with rosmarinic acid by multi-spectroscopic, molecular docking and molecular dynamics simulation approaches. *Food Hydrocolloids, 132*, Article 107895. https://doi.org/10.1016/j.foodhyd.2022.107895

Ma, J. R., Pan, C., Chen, H. M., Chen, Y., Chen, W. J., Pei, J. G., et al. (2023). Interfacial behavior of coconut (Cocos nucifera L.) globulins at different pH: Relation to emulsion stability. *Food Hydrocolloids, 144*, Article 108958. https://doi.org/10.1016/j.foodhyd.2023.108958

Mortele, O., Jorissen, J., Spacova, I., Lebeer, S., van Nuijs, A. L. N., & Hermans, N. (2021). Demonstrating the involvement of an active efflux mechanism in the intestinal absorption of chlorogenic acid and quinic acid using a Caco-2 bidirectional permeability assay. *Food & Function, 12*(1), 417–425. https://doi.org/10.1039/d0fo02629h

Parolia, S., Maley, J., Sammynaiken, R., Green, R., Nickerson, M., & Ghosh, S. (2022). Structure-Functionality of lentil protein-polyphenol conjugates. *Food Chemistry, 367*, Article 130603. https://doi.org/10.1016/j.foodchem.2021.130603

Patil, U., & Benjakul, S. (2017). Characteristics of albumin and globulin from coconut meat and their role in emulsion stability without and with proteolysis. *Food Hydrocolloids, 69*, 220–228. https://doi.org/10.1016/j.foodhyd.2017.02.006

Qi, X., Liu, H., Ren, Y. F., Zhu, Y. H., Wang, Q. L., Zhang, Y. Q., et al. (2023). Effects of combined binding of chlorogenic acid/caffeic acid and gallic acid to trypsin on their synergistic antioxidant activity, enzyme activity and stability. *Food Chemistry: X, 18*, Article 100664. https://doi.org/10.1016/j.fochx.2023.100664

Sadeghi-kaji, S., Shareghi, B., Saboury, A. A., & Farhadian, S. (2019). Spectroscopic and molecular docking studies on the interaction between spermidine and pancreatic elastase. *International Journal of Biological Macromolecules, 131*, 473–483. https://doi.org/10.1016/j.ijbiomac.2019.03.084

Tangsuphoom, N., & Coupland, J. N. (2009). Effect of surface-active stabilizers on the surface properties of coconut milk emulsions. *Food Hydrocolloids, 23*(7), 1801–1809. https://doi.org/10.1016/j.foodhyd.2008.12.002

Tangsuphoom, N., & Coupland, J. N. (2008). Effect of surface-active stabilizers on the microstructure and stability of coconut milk emulsions. *Food Hydrocolloids, 22*, 1233–1242. https://doi.org/10.1016/j.foodhyd.2007.08.002

Tian, Z. Y., Ding, T. L., Niu, H. J., Wang, T., Zhang, Z. Z., Gao, J. H., et al. (2023). 2-Phenylquinoline-polyamine conjugate (QPC): Interaction with bovine serum albumin (BSA). *Spectrochimica Acta. Part A, Molecular and Biomolecular Spectroscopy, 300*, Article 122875. https://doi.org/10.1016/j.saa.2023.122875

Wang, Q. M., Tang, Y. W., Yang, Y. X., Lei, L., Lei, X. J., Zhao, J. C., et al. (2022). Interactions and structural properties of zein/ferulic acid: The effect of calcium chloride. *Food Chemistry, 373*, Article 131489. https://doi.org/10.1016/j.foodchem.2021.131489

Wu, W. N., Wu, Y. Y., Lin, Y., & Shao, P. (2022). Facile fabrication of multifunctional citrus pectin aerogel fortified with cellulose nanofiber as controlled packaging of edible fungi. *Food Chemistry, 374*, Article 131763. https://doi.org/10.1016/j.foodchem.2021.131763

Yu, J., Wang, Y., Li, D., & Wang, L. J. (2022). Freeze-thaw stability and rheological properties of soy protein isolate emulsion gels induced by NaCl. *Food Hydrocolloids, 123*, Article 107113. https://doi.org/10.1016/j.foodhyd.2021.107113

Zhang, L. L., Sahu, I. D., Xu, M., Wang, Y. M., & Hu, X. Y. (2017). Data for beta-lactoglobulin conformational analysis after (-)-epigallocatechin gallate and metal ions binding. *Data in Brief, 10*, 474–477. https://doi.org/10.1016/j.dib.2016.12.021

Zhang, Y. Y., Lu, Y. C., Yang, Y., Li, S. Y., Wang, C., Wang, C. N., et al. (2021). Comparison of non-covalent binding interactions between three whey proteins and chlorogenic acid: Spectroscopic analysis and molecular docking. *Food Bioscience, 41*, Article 101035. https://doi.org/10.1016/j.fbio.2021.101035

Zhao, Q., Wang, Z. N., Yu, Z. X., Gao, Z. Y., Mu, G. Q., & Wu, X. M. (2023). Influence on physical properties and digestive characters of fermented coconut milk with different loading proportion of skimmed coconut drink using Lactiplantibacillus plantarum MWLp-4 from human milk mixing with commercial bacteria. *Food Bioscience, 53*, Article 102598. https://doi.org/10.1016/j.fbio.2023.102598

Zheng, J. B., Gao, Q., Ge, G., Wu, J. H., Tang, C. H., Zhao, M. M., et al. (2022). Dynamic equilibrium of β-conglycinin/lysozyme heteroprotein complex coacervates. *Food Hydrocolloids, 124*, Article 107339. https://doi.org/10.1016/j.foodhyd.2021.107339